Remote Sensing of Environment 112 (2008) 3300–3313

Contents lists available at ScienceDirect

Remote Sensing of Environment

journal homepage: www.elsevier.com/locate/rse

Algal blooming patterns and anomalies in the Mediterranean Sea as derived from the SeaWiFS data set (1998–2003)

Vittorio Barale [a,*], Jean-Michel Jaquet [b,c], Mapathé Ndiaye [c]

[a] Institute for Environment and Sustainability, Joint Research Centre, European Commission, Ispra, Italy
[b] UNEP/DEWA/GRID Europe, Geneva, Switzerland
[c] Remote Sensing and GIS Unit, Earth Sciences Section, University of Geneva, Geneva, Switzerland

ARTICLE INFO

Article history:
Received 3 April 2007
Received in revised form 18 September 2007
Accepted 14 October 2007

Keywords:
Ocean colour
Phytoplankton
Algal bloom
Mediterranean Sea
SeaWiFS

ABSTRACT

Optical remote sensing allows to monitor the space and time heterogeneity of phytoplankton growth in marginal and enclosed seas, a factor critical to understanding their ecosystem dynamics. SeaWiFS-derived (1998–2003) data were used to monitor algal blooming patterns and anomalies in the Mediterranean basin. Yearly and monthly means of chlorophyll-like pigment concentration (*chl*) were computed for the 6 years available, and climatological means derived. The data set statistical variability was assessed by computing yearly and monthly *chl* anomalies, as the difference between each individual year/month and the corresponding climatological year/month. The space and time patterns of the *chl* field appear to concur with the Mediterranean general oceanographic climate, while the *chl* anomalies describe trends and "hotspots" of algal blooming. The analysis shows a general decrease of *chl* values in the yearly and monthly means, an increasing negative trend of *chl* anomalies over the basin interior, and the anticipation of the north-western spring bloom, in comparison to what seen in historical CZCS (1979–1985) data. These have been interpreted as symptoms of an increased nutrient-limitation, resulting from reduced vertical mixing due to a more stable stratification of the basin, in line with the general warming trend of the Mediterranean Sea in the last 25 years. The patterns of high *chl*, coupled to a positive trend of *chl* anomalies, recurring at near-coastal hotspots, appear to be linked to continental runoff and to a growing "biological dynamism" at these sites, *i.e.* to the intensification of noxious or harmful algal blooms, in the north-west, and of coastal fisheries, in the south-east.

1. Introduction

The energy entering ecosystems as sunlight is transferred into chemical energy by photosynthesis, and then propagates through the food web, as a function of inter-relationships among organisms and environmental factors. In aquatic systems, it is phytoplankton — the autotrophic component of the plankton drifting in the water column, including plants and other photosynthetic organisms — that sustains this process. Hence, knowledge of the space and time heterogeneity of phytoplankton growth is critical to understand marine ecosystem dynamics (Mann & Lazier, 2006).

An efficient — and cost-effective — assessment of phytoplankton growth patterns, over basin scales and for multi-annual periods, can only be achieved by means of Earth Observations (EO) in the visible spectral range. In the last three decades, orbital remote sensing of surface optical properties has provided unprecedented views of the abundance and distribution of marine water constituents, and in particular of algal blooming markers such as the concentration of chlorophyll-like pigments (*chl* in the following). Today, the development of so-called "ocean colour" advanced techniques, coupled to the buildup of large-scale, long-term data collections, can be used systematically for characterizing and monitoring the status and trends of marine ecosystems. Future developments in this field are expected to assess phytoplankton species/groups or, more in general, phytoplankton functional types (i.e. conceptual groupings of several phytoplankton species, which are supposed to have in common a given ecological functionality, in terms of either the food web or the biogeochemical cycles) which would have a major impact in biodiversity studies (Alvain et al., 2005).

So far, sizeable times series of historical bio-optical data collected from satellite have been generated by the Coastal Zone Color Scanner (CZCS), from November 1978 to May 1986, and by the *Sea-viewing Wide Field-of-View Sensor* (SeaWiFS), from September 1997 to present. Other orbital sensors that operated in the past, like the *Moderate Optoelectrical Scanner* (MOS), did not have the wide swath needed to ensure quasi-daily coverage of the Earth's surface, or had short-lived (less than 1 year long) missions, like the *Ocean Color and Temperature Scanner* (OCTS), the *Global Imager* (GLI), or the sensors devoted to assess *POLarization and Directionality of the Earth's Reflectances* (POLDER, I/II), failing to provide full seasonal coverage of the oceans.

* Corresponding author. IES, JRC EC, TP 272, 21020 Ispra (VA), Italy. Tel.: +39 0332 789274; fax: +39 0332 789034.
E-mail address: vittorio.barale@jrc.it (V. Barale).

0034-4257/$ – see front matter © 2008 Elsevier Inc. All rights reserved.
doi:10.1016/j.rse.2007.10.014

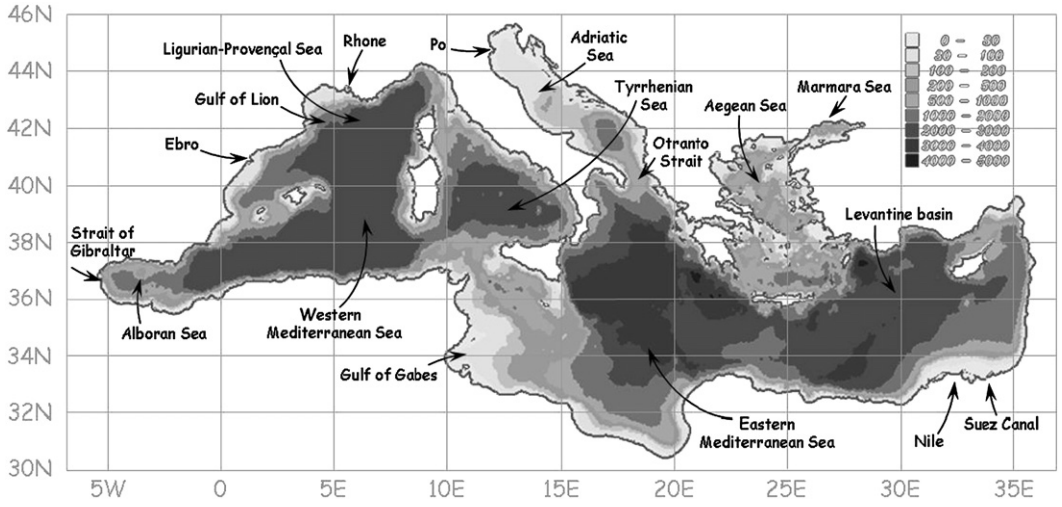

Fig. 1. Mediterranean Sea map, nomenclature & bathymetry (adapted from GEBCO; depths in m).

New quasi-operational sensors, such as the *Moderate Resolution Imaging Spectro-radiometer* (MODIS), *Terra* and *Aqua* versions, and the *MEdium Resolution Imaging Spectrometer* (MERIS), are generating time series of similar data, that will soon be comparable with those of the CZCS and the SeaWiFS. A score of other experimental instruments[1] have also collected, or are still collecting, more limited time series, focusing on the need to address either specific problems or geographical coverage.

In spite of the technical improvements proposed by the successive sensors above, it must be recalled that several limitations still hinder the use of optical remote sensing, especially in near-coastal waters (IOCCG, 2000). This is because of the complexity of separating the various contributions to the spectrum of visible light emerging from the sea surface — which may be due to the diversity of water constituents, or to the morphological setting of the area observed, or to the limitations of the remote sensors' space/time resolution. Uncertainties in the computation of *chl* absolute values can arise primarily owing to the presence, in the water column, of optically active materials other than phytoplankton and related pigments (*i.e.* dissolved organic matter and suspended inorganic particles), with partially overlapping spectral signatures. Further, the depth over which the water-leaving signal — carrying information on these optically active materials — is integrated, is essentially the first optical depth of the water column (that at which the solar irradiance falls to $1/e = 0.37$ of its value just below the surface; Smith, 1981) and can span over 3 orders or magnitude, from cm to dam, depending on the water constituents' nature and concentration. Nevertheless, experience has shown that historical time series of remotely sensed data can provide unique information on phytoplankton growth patterns, and related environmental boundary conditions, to support *in situ* assessments of ecosystem dynamics, with regular observations made over a range of space scales (*i.e.* from a few km to entire basins) and of time scales (*i.e.* from days to years) not available by any other means.

The aim of the present work is to address the topic of recurrent and anomalous algal blooms in marginal and enclosed seas, by using optical remote sensing data. To this end, a time series of data collected by the SeaWiFS mission (McClain et al., 2004) was selected to explore the large-scale, long-term features of the *chl* field in the Mediterranean Sea. Clearly, the results obtained represent only one aspect of the potential to characterize marine ecosystems by means of remote sensing techniques. However, the goal is to indicate how EO strategies can contribute to solve the ecological puzzle presented by the marine environment. In the following, an introduction will be provided to review the main oceanographic traits of the Mediterranean Sea, as well as early attempts of investigating the basin's bio-optical features by means of historical time series of remotely sensed (CZCS) data. Then, the SeaWiFS-derived multi-annual data base, used here to examine the variability of the *chl* field, will be introduced, together with the statistical assessment of the *chl* anomalies derived for the same period. Finally, the space and time patterns emerging from this analysis will be discussed, in light of the Mediterranean oceanographic climate, and the *chl* anomalies will be related to trends and "hotspots" of algal blooming.

1.1. The Mediterranean Sea

The Mediterranean Sea (Fig. 1) — covering an area 2 orders of magnitude below that of the major oceanic basins, and corresponding roughly to 1% of the Earth's surface — can be considered a scale model of the world's oceans (as in *e.g.* Robinson and Golnaraghi, 1995). Although it has limited geographical dimensions, the basin displays a variety of environmental and climatic conditions. The region's seasonal cycle is characterized by a windy, mild, wet winter and by a relatively calm, hot, dry summer. Strong local winds, such as the cold, dry Mistral and Bora, from the north, and the hot, dry Scirocco, from the south, are typical of the region. Substantial mountain ranges border the northern side of the basin, but the corresponding drainage basin is relatively small. And since the southern side is mainly covered by desert, these combined factors tend to limit freshwater input.

Evaporation greatly exceeds precipitation and river runoff, so that the Mediterranean Sea is characterized by very high salinity, a fact that is central to water circulation within the basin (Millot and Taupier-Letage, 2005). Evaporation is especially high in the eastern Mediterranean, causing the water level to decrease and salinity to increase eastward. This pressure gradient pushes cooler, lower-salinity water from the Atlantic Ocean across the entire basin. The relatively less dense Atlantic water flows into the Mediterranean Sea through the Strait of Gibraltar, in the surface layer. This incoming water warms and becomes saltier as it travels east, and is eventually turned into denser Mediterranean water through evaporation. The water sinks to an intermediate depth in the Levantine basin (as well as in the northernmost areas where deep and bottom waters are formed), due to winter cooling, moves back westward and ultimately spills over the sill at Gibraltar, in the bottom layer, and out into the Atlantic Ocean. The complete cycle determines a residence time in the basin of about 80 to 100 years.

[1] A complete list of past, operational and scheduled missions for optical observations of the sea is provided by the International Ocean-Colour Coordinating Group (IOCCG) at http://www.ioccg.org/.

In the Mediterranean Sea, tidal amplitudes are small and the narrow continental shelves prevent tidal amplification along the coast. However, a substantial amount of vertical mixing is provided by strong regional, and seasonal, wind regimes (MEDOC Group, 1970). Dense waters are formed in the Adriatic Sea, due to the effect of the Bora wind blowing from the continent onto the shallow northern basin (Artegiani et al., 1997a,b). The cooling of surface waters increases their density and causes their sinking into the central Adriatic, first, and in the southern Adriatic, later, with episodic outspills over the deep sill of the Otranto Strait. Dense waters, which originates the Western Mediterranean Deep Water, are formed in the Ligurian–Provençal Sea, due to the effect of the Mistral wind, which increases the density of surface waters through intense evaporation and cooling, particularly in the Gulf of Lion region (Gascard, 1973, 1978). This can lead to a complete overturning of the water column, with deep convection processes taking place over 2000 m of water. The vertical mixing ventilates the deepest parts of the Mediterranean Sea, brings deep nutrient-rich waters to the surface and triggers the onset of sizeable algal blooms, sometimes covering the entire north-western basin.

In general, the Mediterranean Sea is nutrient-limited, with consequent low phytoplankton biomass and primary production (Berland et al., 1980). Oligotrophy increases from west to east. By contrast, a rich biodiversity characterizes the Mediterranean ecosystem: the fauna and flora are among the richest in the world, with over 10,000 marine species recorded, highly diverse and with a large proportion (28%) of endemic species (Fredj et al., 1992). No species disappearance has been reported, but changes in species composition and richness have been determined for some areas. The appearance of exotic species — such as that of tropical species from the Red Sea, after the opening of the Suez Canal[2] — is also a growing concern (EEA, 2006a).

The state of Mediterranean open waters is generally good, but many coastal areas are subject to various environmental problems, including eutrophication and heavy-metal, organic and microbial pollution (EEA, 2006a,b). Land-based activities (particularly around the northwestern basin) are considered to be the main sources of pollution. The increasing population of Mediterranean countries, and consequently of related economic activities, places ever more pressure on coastal zones. Since the Mediterranean Sea is mostly oligotrophic, eutrophication is limited largely to specific inshore and adjacent offshore areas. It occurs mostly in enclosed bays (northern Adriatic, Gulf of Lion, northern Aegean) that receive anthropogenically enhanced nutrient loads from rivers and/or the direct discharge of untreated urban and industrial wastewaters. This problem is expected to grow, and is also accompanied by an increasing occurrence of Harmful Algal Blooms (HAB) (Garcés et al., 2000).

1.2. The historical ocean colour data record

In the last two decades, the space and time blooming patterns in the Mediterranean Sea, as related to changes in the ecological balance of the coastal and marine environment, have been investigated repeatedly by monitoring the *chl* field in historical ocean colour data (CZCS, essentially). Statistics of this indicator and its anomalies, as well as comparisons with complementary data collected either from space or *in situ*, were used to highlight "hotspots" for algal blooming in the basin, as well as to address the relationship between local and regional phytoplankton dynamics. Examples of basin-scale assessments are provided by Morel and André (1991) and by Antoine et al. (1995), who looked at algal biomass and primary production in the western and eastern Mediterranean, respectively. Regional assessments have been conducted also for selected sub-basins, characterized by peculiar spatial and/or seasonal variations in the *chl* field, such as the Adriatic Sea (*e.g.* Barale et al., 1986), the Alboran Sea (*e.g.* Arnone et al., 1990), the Levantine sub-basins (*e.g.* Gitelson et al., 1996). More recently, Barale (2003) summarized the analysis of the CZCS-derived climatological data, for a comparison with other satellite data on sea surface temperature and wind speed, collected over the entire Mediterranean Sea in the 1980's and 1990's.

A sample of the CZCS *chl* record (1979–1985) for the Mediterranean Sea, obtained by the Ocean Colour European Archive Network (OCEAN) Project (see Barale et al., 1999; Sturm et al., 1999, for a detailed description of the data set and of the algorithms used to generate it), is shown in the Fig. 2, with the aim of providing an historical reference for the evaluation of the SeaWiFS imagery. The climatological monthly mean images suggest once again the classical geographical subdivisions of the Mediterranean Sea, but propose also an alternative distinction between western and eastern basins, inshore and offshore domains, northern and southern near-coastal areas. The western basin — which could include, in this interpretation, the (northern) Adriatic Sea and Aegean Sea — has higher *chl* values and localized mesotrophic patterns, while the eastern basin has lower *chl* values and a more uniform oligotrophic appearance. Notable features are the Alboran Sea gyre system, generated by water exchange with the Atlantic Ocean; the Ligurian–Provençal Sea enhanced patterns, due to offshore (seasonal) blooming; the Adriatic Sea coastal structures, dominated by the impact of river plumes; the shallow banks in the Gulf of Gabes; and the mesoscale gyres in the Levantine basin, between the islands of Crete and Cyprus.

The climatological monthly means show a seasonal cycle with higher values in the cold season — when continental runoff and vertical mixing are supposed to be the key factors contributing to the nutrients enrichment of surface waters — and lower values in the warm season — due to reduced runoff and to stratification of the water column. This trend is substantially analogous to that shown by the mixed layer depth, as derived from *in situ* measurements (D'Ortenzio et al., 2005). The north-western basin shows instead a sequence of winter low *chl* values (elsewhere referred to as the Gulf of Lions' "blue hole", appearing from January to March) and of massive spring blooms (in April and May), a sequence which has been linked to the Mistral wind seasonal pattern and the convection processes in this region, leading to deep-water formation (Morel & André, 1991; Barale, 2003).

2. Data and methods

2.1. The SeaWiFS-derived chl database

The SeaWiFS-derived database, considered in the present work to examine the recent evolution of *chl* in the Mediterranean Sea, is composed by a time series of individual daily images, of the period 1998–2003, collected whenever favorable meteorological conditions occurred over at least part of the European area. In those cases when two images were collected by the SeaWiFS in the same day, due to the overlap of two consecutive orbits at higher latitudes, only one value per pixel was retained in the processing chain (*i.e.* the value from the scene for which that pixel was observed with the lowest viewing angle). Each of the available images was treated on a pixel-by-pixel basis, to calibrate and correct top-of-the-atmosphere radiances from atmospheric effects, to derive normalized water-leaving radiances and then to compute from these the concentration of water constituents (including *chl*). To this end, the original data were processed using an *ad hoc* algorithm set (Bulgarelli & Mélin, 2000), having common elements with the SeaWiFS Data Analysis System (SeaDAS; Baith et al., 2001), but optimized for applications in the European Seas. Top-of-the-atmosphere un-calibrated images were acquired as full-resolution (1.2 km at nadir) Local Area Coverage (LAC) data, collected by all High Resolution Picture Transmission (HRPT) receiving stations covering the European region. Calibration was performed using the calibration factors provided in Barnes et al. (1999a), with corrections described in Barnes et al. (1999b), and vicarious calibration factors derived from a time series of *in situ* measurements (Zibordi et al., 2006). Geo-location and spectral classification of the

[2] A phenomenon known as the Lessepsian Migration, after Ferdinand de Lesseps, the engineer who oversaw the Canal's construction.

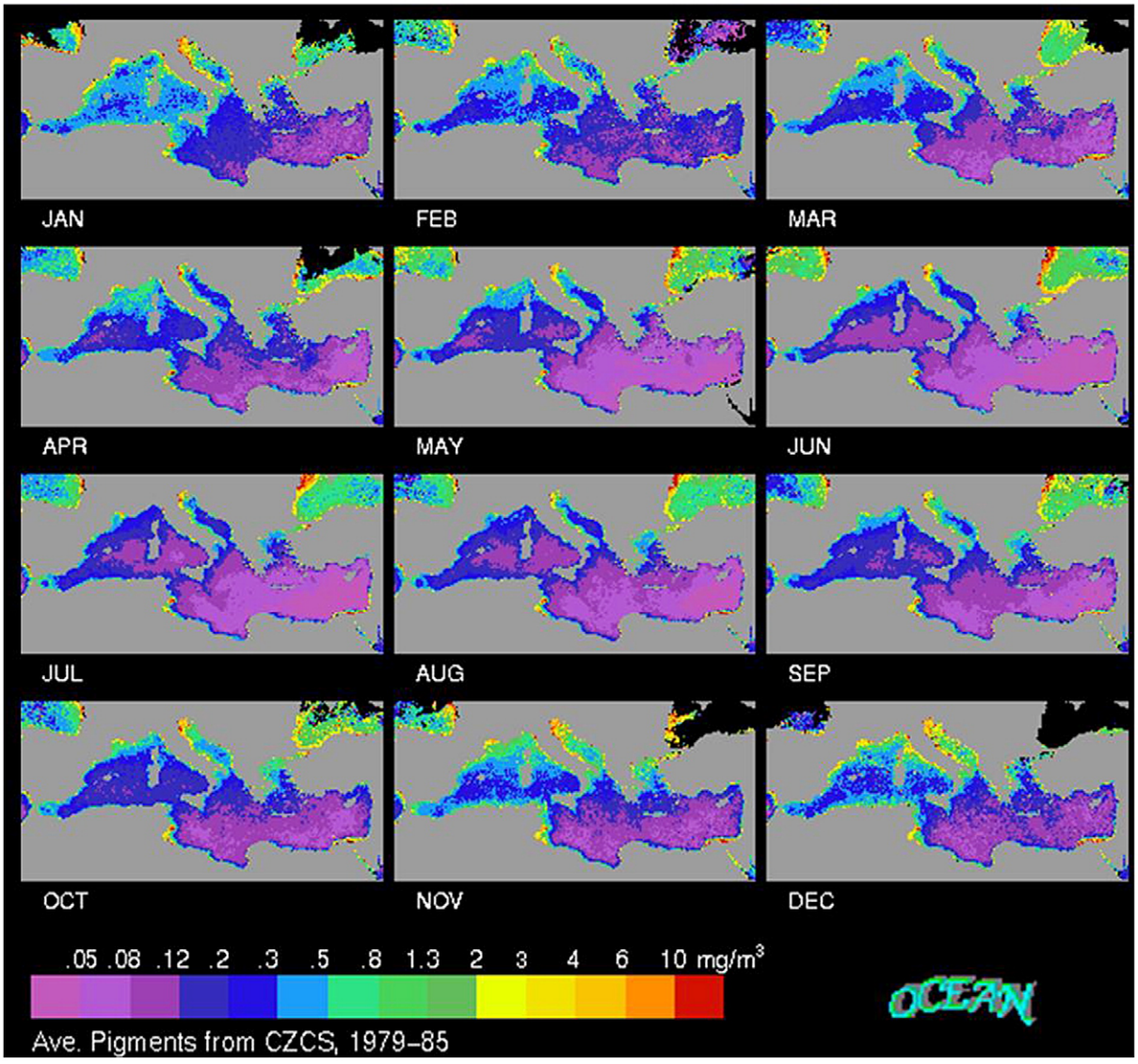

Fig. 2. CZCS-derived (1979–1985) climatological *chl* monthly means, from the OCEAN database, for the Mediterranean Sea.

calibrated top-of-the-atmosphere data were then used to identify the nature of each pixel and flag it accordingly (Mélin et al., 2000). The atmospheric correction scheme used subsequently, for the valid water pixels, is the one implemented by Bulgarelli and Mélin (2000), as detailed in Sturm and Zibordi (2002). In this scheme, the accuracy of producing normalized water-leaving radiances is improved by the combined use of an approximate atmospheric model — accounting for Rayleigh and aerosol multiple scattering, and Rayleigh-aerosol coupling — and of vicarious adjustment factors (in the range of ±3%) for the pre-launch calibration constants of the SeaWiFS channels between 412 and 765 nm, trimming the inaccuracies of both the sensor absolute calibration and the model itself (Bulgarelli et al., 2002). Finally, the computation of *chl* was done using the band-ratio empirical algorithm (OC4) initially proposed by O'Reilly et al. (1998), with revised numerical coefficients, as reported in Mélin et al. (2000). In practice, the relationship:

$$chl = 10\ \exp\left(0.2974 - 2.2429r + 0.8358r^2 - 0.0077r^3\right) - 0.0929$$

where $r = \log_{10}[\rho(\lambda_1)/\rho(\lambda_2)]$ is the log-ratio of the reflectance ρ at the wavelengths $\lambda_1 = 490$ nm and $\lambda_2 = 555$ nm, provides the required estimate of *chl* [mg m^{-3}]. The pixel flag is switched to its turbid water value using both the *chl* estimate and the normalized water-leaving radiance, following the test described by Darzi (1998).

A few caveats concerning the above processing must be recalled here. First, the presence of aerosol, both of anthropogenic and natural origin, and its peculiar composition (*i.e.* industrial emissions, representing about 90% of the aerosol load, and desert dust from northern Africa, constituting the remaining 10%, according to Guerzoni et al., 1999), renders quite difficult the application of standard atmospheric correction schemes to visible imagery of the Mediterranean region. Second, empirical bio-optical algorithms to compute *chl*, based on the inverse dependence between this parameter and the ratio between normalized water-leaving radiances, or reflectances, in the blue and green spectral intervals (such as the ones used in the present case), have been shown to perform significantly worse at regional rather than global scales (Gregg & Casey, 2004). This is particularly true for the Mediterranean basin, due to the problems of atmospheric corrections, as well as to the presence of suspended Saharan dust and particular phytoplankton species (*i.e.* coccolithophores, which have white, highly reflective, calcareous plates) in the water column (Claustre et al., 2002; D'Ortenzio et al., 2002). New SeaWiFS (as well as MODIS and MERIS) algorithms have been presented in the literature for the Alboran Sea (Corsini et al., 2002), the Adriatic Sea (Berthon & Zibordi, 2004), the Gulf of Lion (Ouillon & Petrenko, 2005) and, more recently, the Mediterranean Sea at large (Volpe et al., 2007), which aim at tackling these issues. However, due to the characteristics of the data set

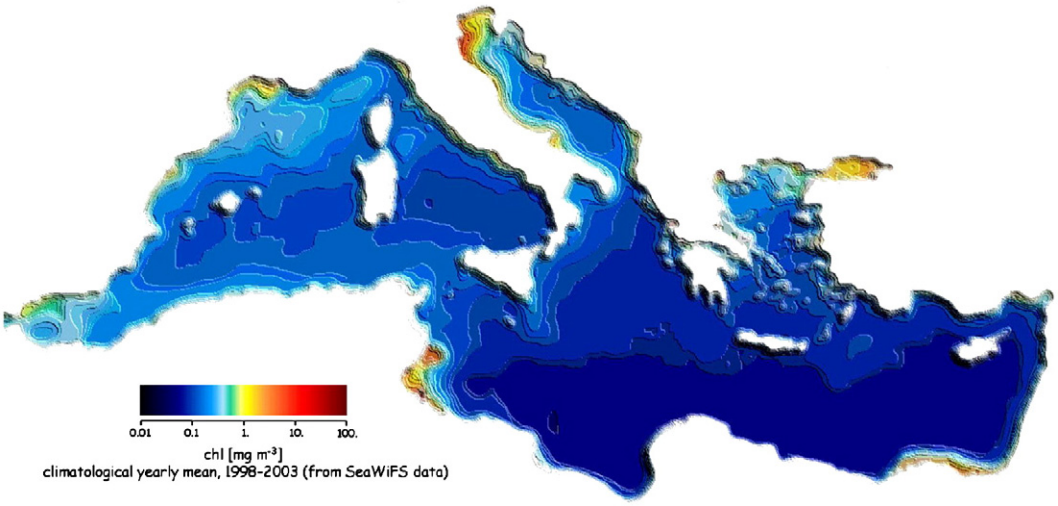

Fig. 3. SeaWiFS-derived (1998–2003) climatological *chl* yearly mean, Mediterranean Sea. Note: a 3D enhancement has been applied to the colour coded data, in order to better highlight *chl* patterns and gradients.

available at the time of the present work, it was chosen to accept the limitations of the standard processing described above, and to concentrate the subsequent data analysis on the evaluation of *chl* relative gradients and patterns.

Once processed, the individual *chl* daily images, in general covering only sections of the Mediterranean area, were re-mapped on a common equal-area (Alber's) projection grid, degrading the original 1.2 km nominal resolution (at nadir) to a uniform 2 km. Image edges, where pixel resolution exceeds 2 km, were excluded from the re-mapping. Starting from the daily *chl* maps, a series of statistical aggregations was derived for the entire 1998–2003 period.[3] Composite *chl* fields, at the yearly and monthly scales, were derived from the re-mapped images by simple time averaging. Climatologies at the yearly scale (Fig. 3) and monthly scale (Fig. 4) were computed as the mean of all (yearly and monthly) composite images available. Further, *chl* anomalies, again at the yearly and monthly scales, were computed as the difference between each yearly/monthly mean and the climatological year/month. All SeaWiFS-derived images presented in the following are coded using the same colour bar (representing *chl* values in mg m^{-3}; anomalies are coded using a two-colour bar, blue for negative and red for positive values, also representing *chl* values in mg m^{-3}), so that they are directly comparable from both the geographical and the quantitative point of view. Numbers along the horizontal and vertical axis of the images, when present, show longitude and latitude values, respectively.

The main patterns emerging in the SeaWiFS data record are reminiscent of those already noted for the CZCS 1979–1985 climatology. From the quantitative point of view, keeping in mind the above limitations of the bio-optical algorithms adopted here, variations in *chl* were expected because of the differences in the sensors' characteristics and calibration (performed *a posteriori* in the CZCS case), as well as in the processing algorithms. Those used for SeaWiFS showed, in particular, an improved performance, with respect to those used for CZCS, which tended to overestimate *chl* in winter (due to low sun elevation angles and consequent multiple scattering effects), in the blue band in particular, and further to overestimate *chl* in near-coastal waters, where optically active materials other than chlorophyll-like pigments may contribute to water optical properties (Antoine et al., 1995). A methodical, quantitative inter-comparison of CZCS and SeaWiFS data, and of data from other sensors as well, has been conducted by Bricaud et al. (2002). In the present case, the SeaWiFS-derived *chl* values appear to be systematically lower than, but geographically consistent with the OCEAN climatological means, shown in Fig. 2. The main differences occur in the north-western (and westernmost) part of the basin, where more intense blooming seems to have occurred in the period considered here. Overall, the results obtained are very similar to those described in earlier analyses that used a shorter time series of SeaWiFS data (see *e.g.* Bosc et al., 2004).

2.2. Statistical analysis of the chl anomalies

The work presented here focuses on a statistical approach to the analysis of the 72 *chl* monthly anomaly maps available. To this end, data from the Mediterranean proper were extracted from the images, discarding pixels from other water bodies as well as shallow-water coastal pixels. Following earlier studies on the influence of bottom reflectance on the *chl* signal (Jaquet et al., 1999), pixels with a depth equal or shallower than 30 m were eliminated by means of a mask derived from the General Bathymetric Chart of the Oceans (GEBCO) data set[4], suitably geo-referenced to the same *chl* map projection. The resulting monthly anomaly (reduced) maps were further analyzed, in order to quality-check the data (for distribution type, outliers, "anomalous" values within the anomalies, *etc.*), and then to evaluate spatial structures and temporal trends.

In general, the statistical distributions of the *chl* monthly anomalies are characterized by a wide dispersion. The examination of the 72 histograms showed a variety of distributions, either symmetrical, with varying degrees of peakedness, skewed, or polymodal. The spatial auto-correlation analysis indicated a non-random nature of the series variability. Further, the variations appeared to be definitively periodic, over the annual cycle, with higher values in summer than in winter. This hypothesis was tested by computing the correlogram of the spatial auto-correlation time series, as well as its Fourier spectrum. In both cases, there is a significant major peak at a frequency close to 6 and 12 months. More details on the statistical characteristics of the *chl* monthly anomalies data set can be found in Barale et al. (2005).

The chronological evolution of the monthly anomalies was studied by means of a pixel-by-pixel linear fit to the images, and then by considering intercepts, slopes, correlation coefficients and number of

[3] Details on data set composition at http://oceancolour.jrc.ec.europa.eu/ & http://emis.jrc.ec.europa.eu/.

[4] Details and complete data set available at http://www.ngdc.noaa.gov/mgg/gebco/grid/1mingrid.html.

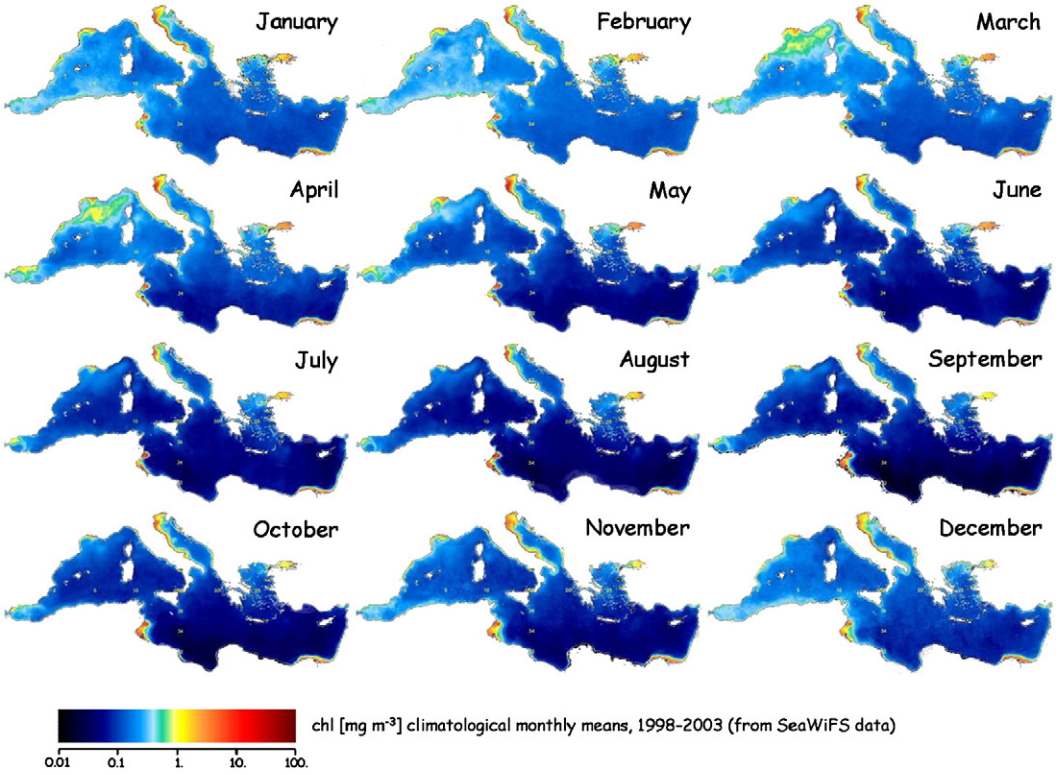

Fig. 4. SeaWiFS-derived (1998–2003) climatological *chl* monthly means, for the Mediterranean Sea.

samples (used to compute the significance level of the correlation coefficient). Prior to the computation, monthly anomalies expressed in absolute values (mg m^{-3}) were converted in % values, in order to enhance existing trends even in the case of weaker anomalies. Fig. 5 shows an example of the regressions which have been computed on each of the 1,653,340 pixels composing the (reduced) anomaly maps. The trend parameters obtained for each pixel (*i.e.* intercept, slope, correlation coefficient, number of samples) were mapped again on the same geographical grid (Fig. 6). The maps of the intercepts *i* and slopes *s* are characterized by non-random patterns. In spite of some noise, positive and negative values cluster in regions, indicating common evolution trends. The *i* and *s* features are somewhat correlated across both maps: negative intercepts mostly coincide with positive slopes (see *e.g.* the Alboran Sea, as well as the Balearic–Provençal–Ligurian Sea, in the western basin; the north-western Adriatic Sea and the north-eastern Aegean sea; the areas south and east of Crete as well as offshore the Egyptian–Israeli–Lebanese coast, in the eastern basin) and vice-versa. The significance of the *i* and *s* patterns can be evaluated from the maps of the correlation coefficients *r* and number of samples *n* shown in Fig. 6. From the latter, it can be seen that *n* is predominantly higher than 65 (maximum 72). For this value of *n*, the 95% significance level for *r* is 0.25 (0.32 for 99%). Hence, based on the

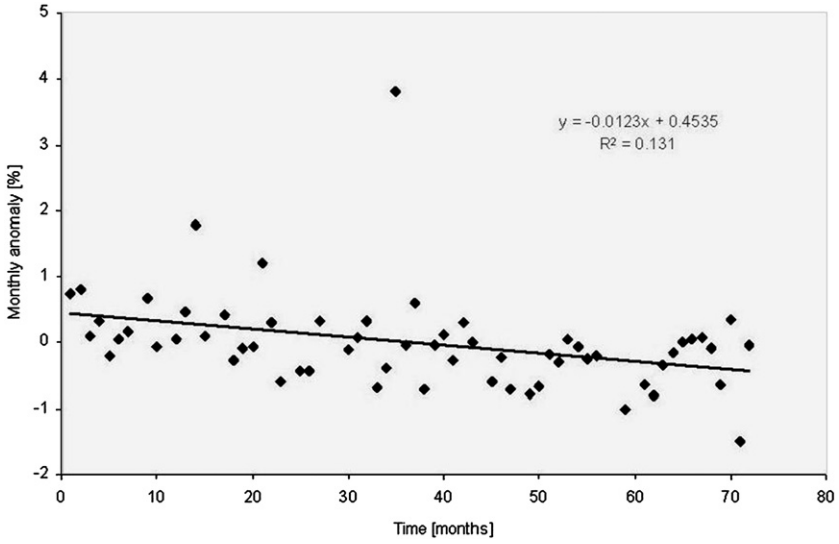

Fig. 5. Chronological evolution of the SeaWiFS-derived *chl* monthly anomalies, converted into % values, at a given point of the Mediterranean Sea geographical grid, with corresponding linear regression. Intercept, slope and correlation coefficient of the linear fit are reported in the upper right quadrant.

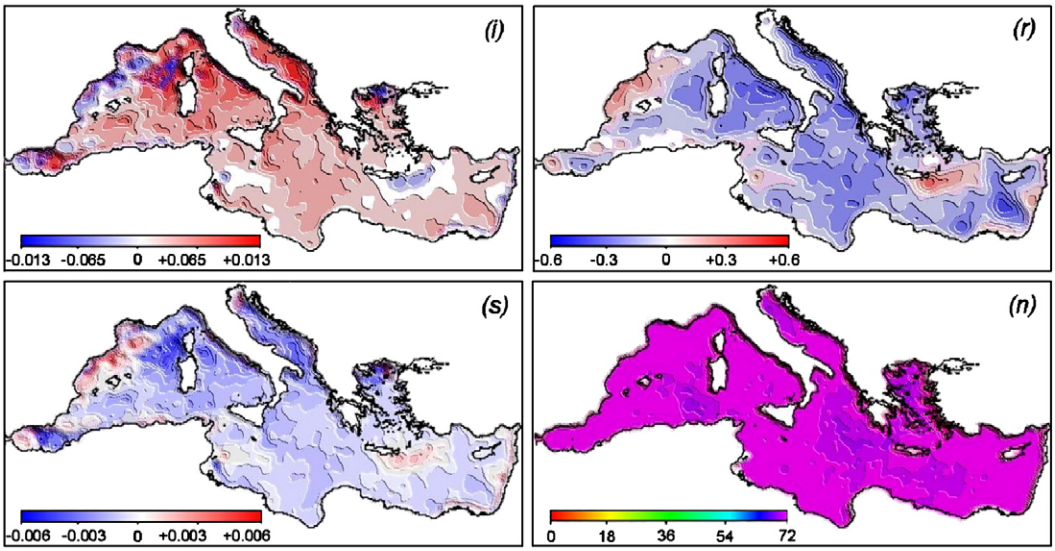

Fig. 6. Intercept (*i*), slope (*s*), correlation coefficient (*r*) and number of samples (*n*), derived on a pixel-by-pixel basis from the linear regression analysis of the SeaWiFS-derived *chl* monthly anomalies (expressed as % values), for the entire Mediterranean Sea. Note: a 3D enhancement has been applied to the colour coded data, in order to better highlight patterns and gradients and the parameters shown.

map in Fig. 6, panel (*r*), both *i* and *s* trends are significant in the areas where *r* is colour coded as mid-to-dark blue and mid-to-dark red.

3. Results and discussion

3.1. Space and time patterns in the SeaWiFS-derived chl composites

The oligotrophic character of the basin — and of the Levantine, in particular — is the main feature of the Mediterranean Sea appearing in the climatological annual mean of Fig. 3. The western and eastern basins are not too dissimilar, in the offshore (pelagic) domain, with an overall basin average of *chl* around 0.2 mg m^{-3}. The inshore (near-coastal) domain, on the other hand, presents higher *chl* values in the north-west and west, and lower *chl* values in the south and south-east. The high-*chl* near-coastal areas include the Balearic–Provençal–Ligurian sub-basins, and the (northern) Adriatic and Aegean Seas. This rim of enhanced pigments, around most of the northern Mediterranean, is linked to the impact of (fluvial) runoff from continental margins (*i.e.* both a direct impact due to the sediment load and one induced on the plankton flora by the associated nutrient load), but has been associated also with the vertical mixing regime due to the prevailing winds, *i.e.* the Mistral in the north-west, the Bora over the Adriatic and the Etesians over the Aegean (Barale & Zin, 2000).

Other examples of dynamical features related to mixing processes in the water column are provided by the quasi-permanent gyres due to the incoming Atlantic jet in the Alboran Sea, or by the giant filament of Capo Passero, at the southern tip of Sicily, also linked to the current system originated by the Atlantic jet flowing eastward over a steep continental slope. Where major rivers (*i.e.* the Ebro, Rhone, Po, in the western basin and the Nile, in the eastern basin) flow into the basin, the coastal area appears to be permanently under the direct influence of their plumes, a feature that was already evident in the CZCS historical data set (Barale & Larkin, 1998). Minor river discharges, or non-point sources of runoff, also have a coastal signature in the pigment field, as along the Italian coast in the Tyrrhenian Sea, along both the Italian and Albanian coastlines in the Adriatic Sea, and along the northern shores of the Aegean Sea and the Marmara Sea, where exchanges with the Black Sea take place. In the Gulf of Gabes, around the islands of Kerkenna and Djerba, instead, the enhanced pigment signal appears to be an artifact, due to direct bottom reflection in areas of shallow clear waters, and not to coastal runoff patterns (except perhaps in direct connection with the Gabes urban area; Jaquet et al., 1999).

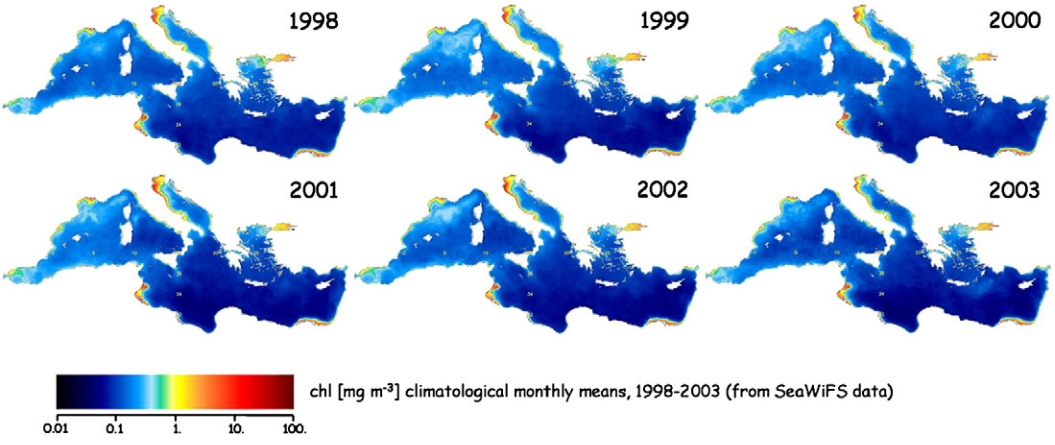

Fig. 7. SeaWiFS-derived (1998–2003) *chl* yearly means for the Mediterranean Sea.

The features of the climatological yearly mean image are recurrent in the single yearly means of Fig. 7. However, a certain degree of inter-annual variability is evident in the main spatial patterns. In particular, the size of the blooming area in the northwestern sub-basin (with $chl \geq 0.3$ mg m^{-3}) appears to increase from 1998 to 1999, but then to decrease from 2000 to 2003. Similarly, the size of the super-oligotrophic area in the south-eastern sub-basin (with $chl \ll 0.1$ mg m^{-3}) appears to increase in the second half of the period covered. Taking in due consideration the caveats on absolute values introduced in the previous section, the *chl* average basin value derived from the yearly means (*i.e.* a single *chl* value computed as the total average of all pixels composing each yearly image) is rather constant over the whole period considered (*i.e.* 0.2 ± 0.01 mg m^{-3}), even though it seems to present a slight decrease in the last 3 years.

The spatial patterns appearing in the climatological monthly means of Fig. 4 are not dissimilar from those observed at the annual scale, but show enhancements over variable seasonal periods. The whole Mediterranean Sea presents higher *chl* values in January, February and March (period referred to as winter, in the following), with peak blooming occurring earlier (February) in a few sub-basins and current systems (*e.g.* the Alboran Sea and the Algerian Current, in the western basin), or later on (March) in others (*e.g.* the Ligurian–Provençal Sea, in the western basin, but also the north-eastern Levantine basin, in correspondence to the Rhodes Gyre). While blooming continues in a few areas (*i.e.* the north-west, but also the Alboran Sea) in April, May and June (spring, in the following), signs of oligotrophic conditions appear in the eastern basin as early as March (but as late as June in the west, *i.e.* in the Tyrrhenian Sea). The oligotrophic state prevails in July, August and September (summer), everywhere in the eastern basin, except for coastal plumes, and in the interior of the western basin. Elsewhere in the western basin, the northern near-coastal area of the Ligurian–Provençal Sea seems to retain higher *chl* values even in summer, similarly to the southern near-coastal area impacted by the incoming (permanent) Atlantic jet. These conditions appear to relax in October, November and December (fall), as early as October in the western basin, starting from the south-west, but only in December in the eastern one, when blooming seems to take up again, in preparation for the winter peak.

In the preceding analysis, the SeaWiFS-derived time series presents a seasonal cycle analogous to the one appearing in the historical CZCS data set, *i.e.* a bimodal pattern with *maxima* in the colder season, from late fall to early spring, followed by *minima* in the warmer one, from late spring to early fall. This is substantiated by the fluctuation of the average basin value of *chl* derived from the monthly means (*i.e.* a single *chl* value computed, again, as the total average of all pixels composing each monthly image), shown in Fig. 8 (left panel). As noted already for the annual means, the *chl* indicator seems to present a decreasing trend, over the period covered, estimated (by linear regression) to be about 20% of the climatological average value for the entire basin.

The climatological seasonal trend (Fig. 8, right panel), obtained by computing an average basin value of the *chl* indicator from the climatological monthly mean images, suggests that the Mediterranean Sea as a whole presents a behavior similar to that of a sub-tropical basin, where the light level is never a limiting factor, so that its decrease in winter does not inhibit algal growth, but the nutrient level always is. In such a scenario, higher *chl* values would occur in the colder, windy and wet (winter) season, and would be related to the biological enrichment of surface waters due to surface cooling, vertical mixing and continental runoff — as opposed to lower *chl* values occurring in the warmer, calm and dry (summer) season, when the water column is strongly stratified and no nutrient supply, from coastal zones or deeper layers, is readily available.

Unlike what is seen in the sequence of *chl* average basin values, derived from the historical CZCS climatological monthly means (Barale & Zin, 2000), the curve of Fig. 8, right panel, does not present absolute *maxima* in January and in (November and) December. Peak *chl* values now occur in February and March, with reduced values in January and in December. Hence, the SeaWiFS-derived climatological seasonal cycle shows that, after the summer low, *chl* grows in fall, reaches its absolute *maximum* in the middle of winter, and then decreases again in spring, toward its summer *minimum*. This does not affect the general validity of the sub-tropical scenario, described earlier when considering the cycle of the entire Mediterranean basin, but points to the fact that some regions, namely the western sub-basins, have a somewhat different seasonality. The difference is so pronounced, in fact, that it affects basin statistics, when integrated *chl* values are considered to summarize the behavior of the basin as a whole.

The inter-annual variability of this seasonal cycle is illustrated in Fig. 9, where the *chl* average basin values from the monthly means, subdivided in winter (panel a) spring (panel b), summer (panel c) and fall (panel d), are plotted against time. The winter plot shows that the highest value can be reached already in January, and then maintained in the following months (as in 1998, 2000 and 2002), but it can also be delayed to February (as in 2001) or even to March (as in 1999 and 2003). In spring, *chl* drops rapidly from winter to summer levels. The summer plot shows that the lowest values are reached in August (the only exceptions occurring in 2000 and even more so in 2001), but that it varies very little throughout the entire season. In fall, the values rise, again rather systematically, from summer to winter levels. Seasonal excursion of *chl*, in a given year, can be on the order of 10–20% in winter; as high as 20–40% in spring, the largest observed; only 10% in summer; and then 20–30% in fall.

While the Mediterranean basin as a whole seems to follow such a model, significant departures occur in some areas, and in particular in

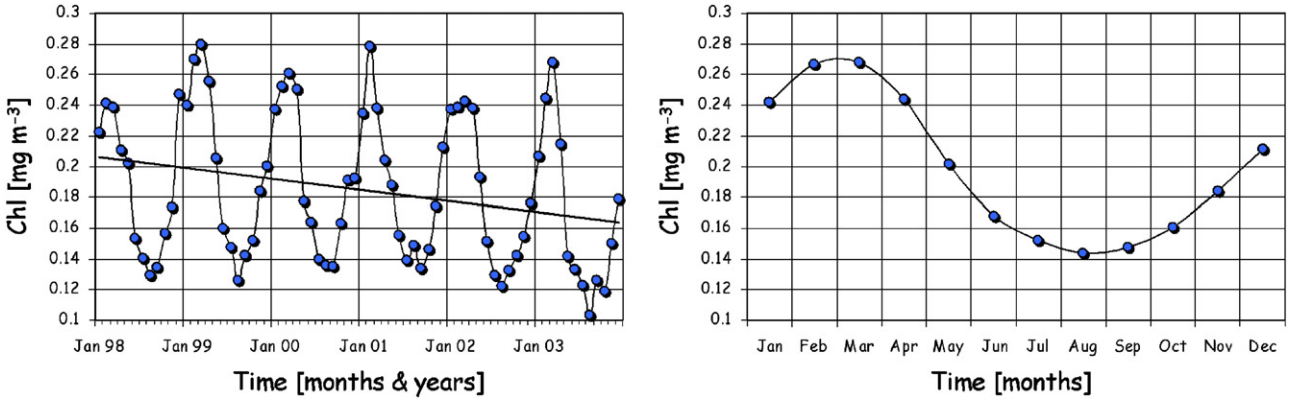

Fig. 8. Time variations of the SeaWiFS-derived *chl* average basin value, computed from the 72 monthly means, with linear fit (left panel), and from the 12 climatological monthly means (right panel), for the Mediterranean Sea.

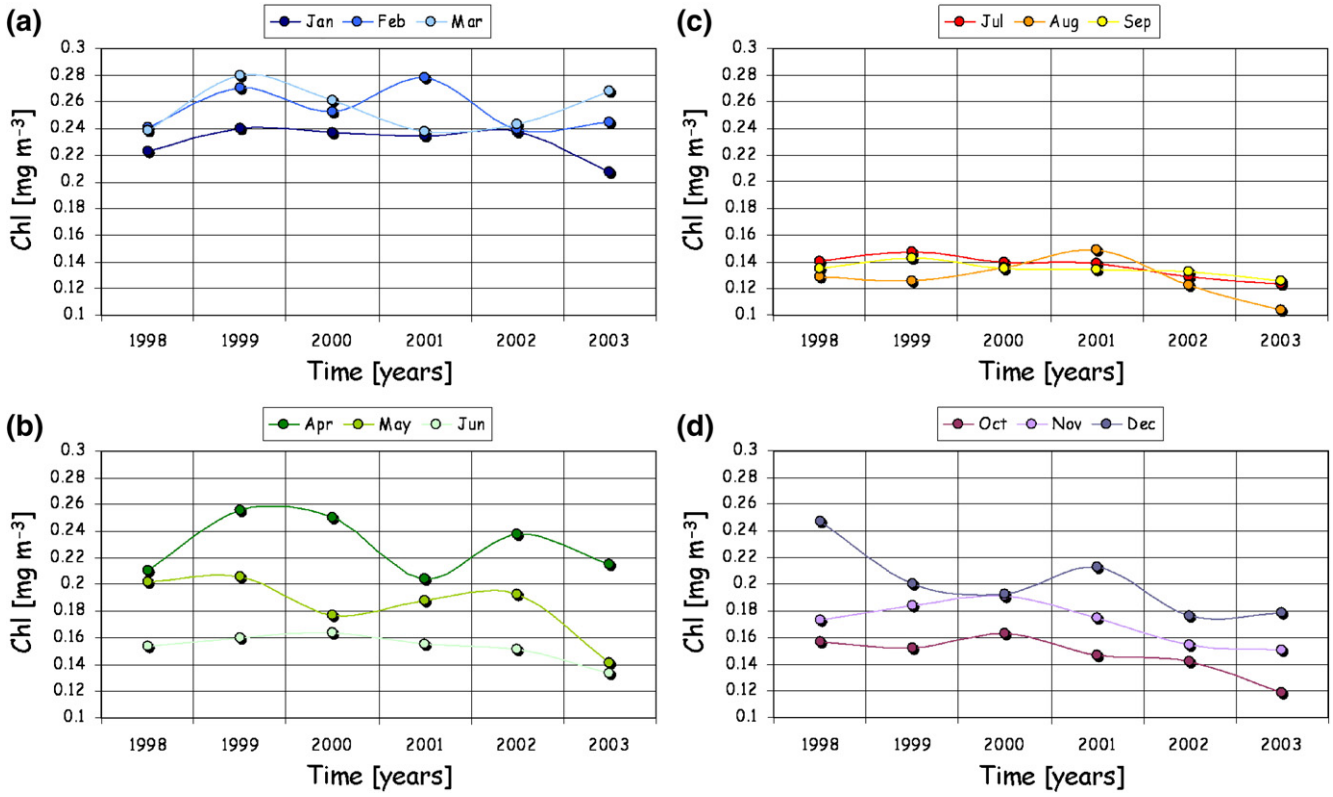

Fig. 9. Inter-annual variability of the SeaWiFS-derived *chl* average basin value, computed from the monthly means, in winter (panel a), spring (panel b), summer (panel c) and fall (panel d), for the Mediterranean Sea.

the northern sub-basins. Notably, the Adriatic Sea and the Aegean Sea display a late winter and, mostly, early spring (April) enhancement in *chl* values, superimposed to the general annual trend. Local conditions describing a combination of seasonal signatures can be recognized also elsewhere, in both the western basin — where the Alboran Sea *e.g.* presents the additional feature of coastal *chl* enhancement in early spring — and in the eastern basin — where the Rhodes Gyre core, after reaching a late winter (March) *chl* maximum, maintains its characteristics throughout the year, even appearing in summer months as the only, isolated, offshore spot of high *chl* in the super-oligotrophic basin.

The Ligurian–Provençal Sea deserves a special reference, in this list of exceptions, for displaying, primarily in the Gulf of Lion, a rather different, almost opposite, seasonal cycle. In fact, the lowest *chl* values appear in winter, and are followed by a massive bloom in March and April. This feature, the most pronounced of the entire Mediterranean Sea, continues to be identifiable even throughout summer and fall. In this area, the lower *chl* values of the winter season are originated when strong northerly Mistral winds blow from the continental landmass onto the sea, so that the resulting deep convection processes, triggered systematically by this particular wind regime, can mix surface waters down to 1500–2000 m of depth. This seems to be particularly true for the Lion Gyre, an area of deep-water formation — *i.e.* the so-called "blue hole" already seen in the historical CZCS data set — where the lack of high *chl* in winter is linked to the extreme conditions generated by the overturning of the entire water column. This seasonality would be closer to that of a sub-polar basin, rather than a sub-tropical one, with lower pigment concentration in winter, because of reduced light or actually, more important in this case, because of the deep vertical mixing and turbulence due to the prevailing wind field, which prevents algae to be stabilized in the upper well-lit layers. The ensuing spring bloom, then, would be triggered by the relaxation of these conditions, when the wind field reduces its impact, the water column — enriched in nutrient content by the prolonged period of deep convection — becomes sufficiently stable, and stratification occurs in the sub-basin (Levy et al., 1998, 1999, 2000).

It must be noted, however, that the period of deep convection appears to be shorter than in the CZCS climatological sequence (see Fig. 3), where the monthly mean images showed a larger "blue hole", extending also in the Ligurian Current region, from late fall to early spring (an occurrence noticed also by Bosc et al., 2004). This feature — occurring in the historical CZCS data as early as December, and then most intensely in January, February and March as well — in Fig. 4 can hardly be recognized in December, starts to become evident in January, and is obvious only in February, while extensive blooming takes place already in March. Interestingly enough, no "blue hole" was visible in the imagery of fall of 1997 (not shown here), when the SeaWiFS time series got started. This apparent lack of deep convection in the Gulf of Lion, was followed in 1998 by the least pronounced and shortest spring bloom observed in the same area for the 6 years considered. This testifies once more the importance of wind-induced processes in the biological cycles of the northwestern Mediterranean Sea, where the enrichment of surface waters supports a large biomass of primary (and secondary) producers, as well as a highly developed food web — including a sizeable standing population of fin whales, *Balaenoptera physalus*, and various other marine mammals (see *e.g.* Forcada et al., 1996, and references therein).

3.2. Blooming anomalies

The SeaWiFS-derived *chl* anomaly maps highlight the geographical spread and intensity of blooming patterns, which differed in each period from the corresponding climatological mean. The series shows that anomalies can occur just about anywhere in the basin, even though they tend to recur in areas of intense blooming, and in all periods of the year. In the sequence of *chl* yearly anomalies (Fig. 10), the whole Mediterranean basin shows mostly positive anomalies in the first 3 years and mostly negative anomalies in the second 3 years.

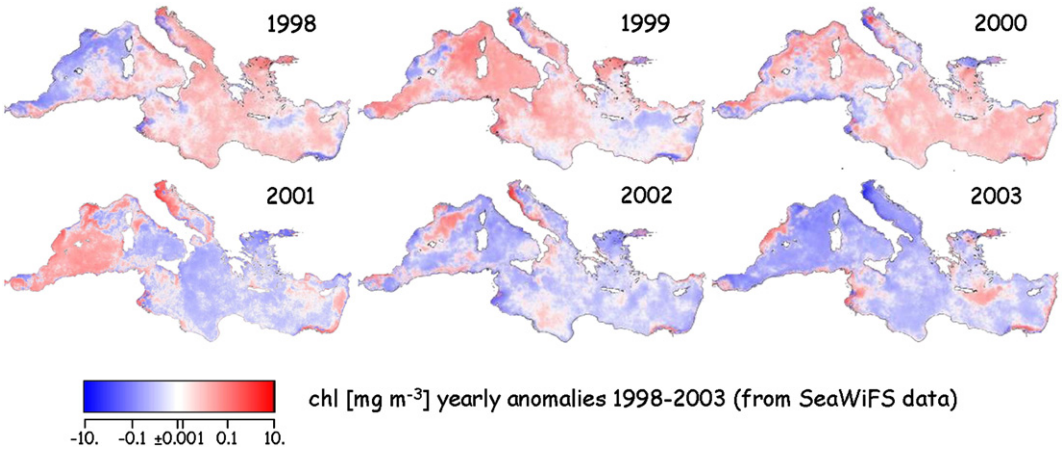

Fig. 10. SeaWiFS-derived (1998–2003) *chl* yearly anomalies, for the Mediterranean Sea.

The north-western sub-basin displays a *quasi* systematic counter-trend, with respect to the remainder of the western basin, both in a negative sense, as in 1998–1999, as well as in a positive sense, as in 2002. The Levantine sub-basin also seems to show a recurring counter-trend, with respect to the eastern basin, again both in a negative sense, as in 1998–1999, as well as in a positive sense, as in 2003. Near-coastal areas can also present sharp fluctuations (absolute value ≥0.1 mg m^{-3}) from negative to positive anomalies, and *vice versa*, as apparent along the Catalan coast or in the northern Adriatic sea (see *e.g.* 1998 *vs* 2003, in both cases). Very high anomalies (absolute value ≥10 mg m^{-3}) are seen to recur only alongshore, in shallow waters (*e.g.* near the Gulf of Gabes) or around river plumes (*e.g.* near the Po river delta).

In the sequence of 72 *chl* monthly anomalies (not shown here; see Barale et al., 2004; samples in Fig. 11), there are at least three main types of anomalies, which seem to be of particular interest. The first is a basin-wide anomaly, when the greater part of the Mediterranean basin appears to be above or below the climatological mean value (*e.g.* December 1998, positive; December 2002, negative). The second kind of anomaly shows the western and the eastern basins oscillating in opposite ways (*e.g.* September 2000, western basin mainly negative, eastern mainly positive; and February 2001, opposite situation). In general, though, the most common anomalies are of a third kind, which involves only a specific sub-basin or near-coastal area. In the western basin, the Alboran Gyres and Algerian Current system, and even more prominently the Ligurian–Provençal Sea, where the most intense blooming takes place, are the main sites of these recurring local anomalies. As an example, both positive and negative anomalies can be seen, in sequence, between February and March 1998 in these areas. In the eastern basin, the gyre system south and east of the Island of Crete (the Rhodes Gyre, in particular) and, somewhat surprisingly, the Egyptian–Israeli–Lebanese coastal area displays similar characteristics (*e.g.* negative anomalies in March 1998, and positive in February 2001).

3.3. Trends and "hotspots" of anomalous algal blooming

The linear regression parameters shown in Fig. 6 provide information about the general trend of the monthly *chl* anomalies. Considering the first derivative of the linear fit associated with each pixel (*i.e.* the map in Fig. 6, parameter *s*), most of the Mediterranean area shows negative slopes, with positive intercepts, suggesting that, between 1998 and 2003, anomalies were getting smaller and smaller over the largest part of the basin interior. In some small areas, as in the easternmost marginal area of the Ligurian–Provençal Sea, negative slopes are even accompanied by negative intercepts. Given that the regressions concern % anomalies, this implies an attenuation of the blooming patterns' intensity almost everywhere in the basin, in good agreement with the general decrease of the *chl* average basin value already seen in the yearly and monthly means.

Other areas show a counter-trend of positive slopes, with negative intercepts, associated, in the original SeaWiFS imagery, to pelagic eddy-like structures (*e.g.* in the Gulf of Lion, in the Alboran Sea and along the Algerian current, in the west; in the region south-east of Crete, in the east), or to extensive coastal plumes (*e.g.* along the Catalan coast, in the northern Adriatic Sea and Aegean Sea, and along the Egyptian–Israeli–Lebanese coast). In the case of open water gyres, as the Lion Gyre and the Rhodes Gyre, the positive anomalies are likely

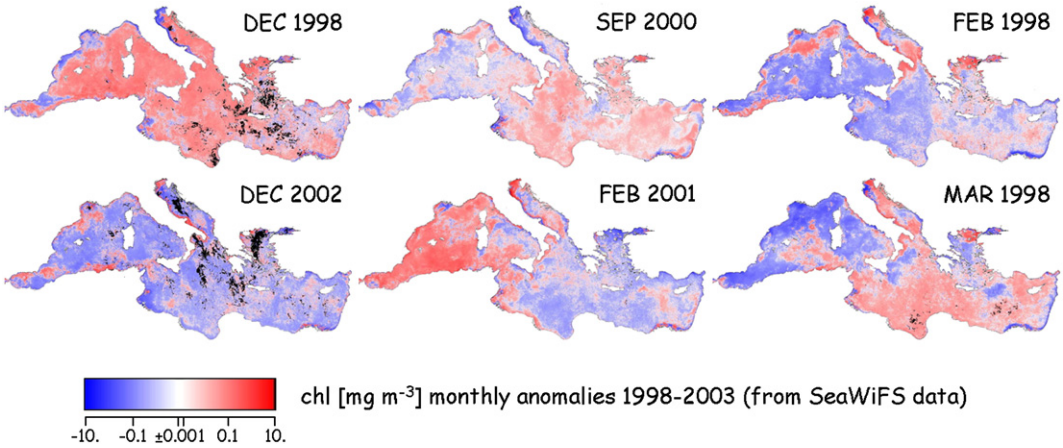

Fig. 11. Selected SeaWiFS-derived (1998–2003) *chl* monthly anomalies, for the Mediterranean Sea.

to reflect enhanced air–sea interactions due to the major wind patterns of these regions (*i.e.* the Mistral and the Etesian winds, respectively; see *e.g.* Zecchetto and Cappa, 2001). Interestingly enough, *chl* anomalies in the Gulf of Lion have been mostly negative after winters in which the so-called "blue hole" — indicative of strong deep convection processes — did not develop or appeared to be weaker (*e.g.* the 1997–1998 fall and winter). Instead, increasingly positive anomalies characterized the greater part of the period, in which it can be safely assumed that strong vertical mixing, with consequent enrichment of the surface layer by deep nutrients, left a clear mark first in a well developed "blue hole" and then in the extensive blooming patterns.

Two coastal areas, in the north-western and the south-eastern Mediterranean Sea, emerge as outstanding "hotspots" for anomalous algal blooming. In both cases, along the Catalan coast and the Egyptian–Israeli–Lebanese coast, the *chl* anomalies were seemingly getting larger and larger, in the period considered — in parallel to a growing "biological dynamism" at these sites (*i.e.* the intensification of noxious or harmful blooms in the north-west and the increased yield of coastal fisheries, in the south-east; see below). These hotspots present a number of similarities: large nutrient sources of continental origin; patterns of high water constituents concentrations, rooted at special coastal (urban) sites; strong current systems, inducing the offshore spreading of coastal plumes. In both cases, point sources of runoff are scattered all along the coast; however, the main nutrient supply is upstream in the Levantine case (*i.e.* the Nile river delta), downstream in the Catalan case (*i.e.* the Ebro river delta). Further, the high-*chl* features off the south-eastern coast are sharper, better recognizable against an oligotrophic background, while those off the north-western coast have more diffused appearance and sometimes merge with co-varying offshore patterns.

3.4. Algal blooming "hotspots" and biomass/biodiversity variations

The near-coastal, mesotrophic region in the north-western Mediterranean Sea, which appears here as one of the main hotspots for *chl* anomalies in the basin, has experienced in recent years an increase in the emergence and blooming of alien species (Vila & Masó, 2005). This increase in biodiversity, with its negative twist due to the growing incidence of HABs, is best exemplified by the increasing blooming episodes of *Alexandrium*, the dinoflagellate *genus* which causes most noxious or harmful blooms in the basin (Garcés et al., 2000). Various species of *Alexandrium* (*A. minutum, A. catenella, A. taylori*) have been recorded in the north-western Mediterranean, in particular at several sites along the Catalan shores, where blooming takes place primarily at coastal sites (Vila et al., 2001). Although a significant body of information exists on recurring *Alexandrium* blooms at local scales, in some cases it is difficult to demonstrate whether such blooms start in confined waters, or stem from episodes occurring in open waters, just on the basis of *in situ* studies (Vila et al., 2005). Furthermore, if a bloom starts in confined waters, it is not clear whether, and under what circumstances, it can then be exported to open waters. What appears to be most critical, in order to assess biodiversity trends, is to determine if there is any relationship between inshore HAB events — of some target species, imported via ships' ballast waters, such as those of the *Alexandrium* genus — and the large-scale, long-term endemic offshore events, observed in the satellite imagery. The SeaWiFS data used here to trace phytoplankton dynamics at the regional scale, and for a multi-annual period, seems to provide frequent examples of the decoupling between inshore and offshore regimes, even in those cases when they seem to co-vary (as *e.g.* in Fig. 12). The blooms observed in the imagery along the Catalan coast appear to be confined to the near-coastal zone and to be separated from the offshore regional patterns, suggesting that the forcing functions of the two kinds of events are different, or overlap only marginally.

The near-coastal, oligotrophic region in the south-eastern Mediterranean Sea, finally, may well represent the ultimate case of anthropogenic impact on near-coastal areas. Whereas the Levantine basin is known as the marine equivalent of a terrestrial desert, sizeable high-*chl* filaments and plumes originating from the Egyptian–Israeli–Lebanese coastal area are evident in the entire SeaWiFS data set (Weber et al., 2004).

The origin of such features can be related to coastal runoff, and not to coastal upwelling, on the basis of a surface temperature higher,

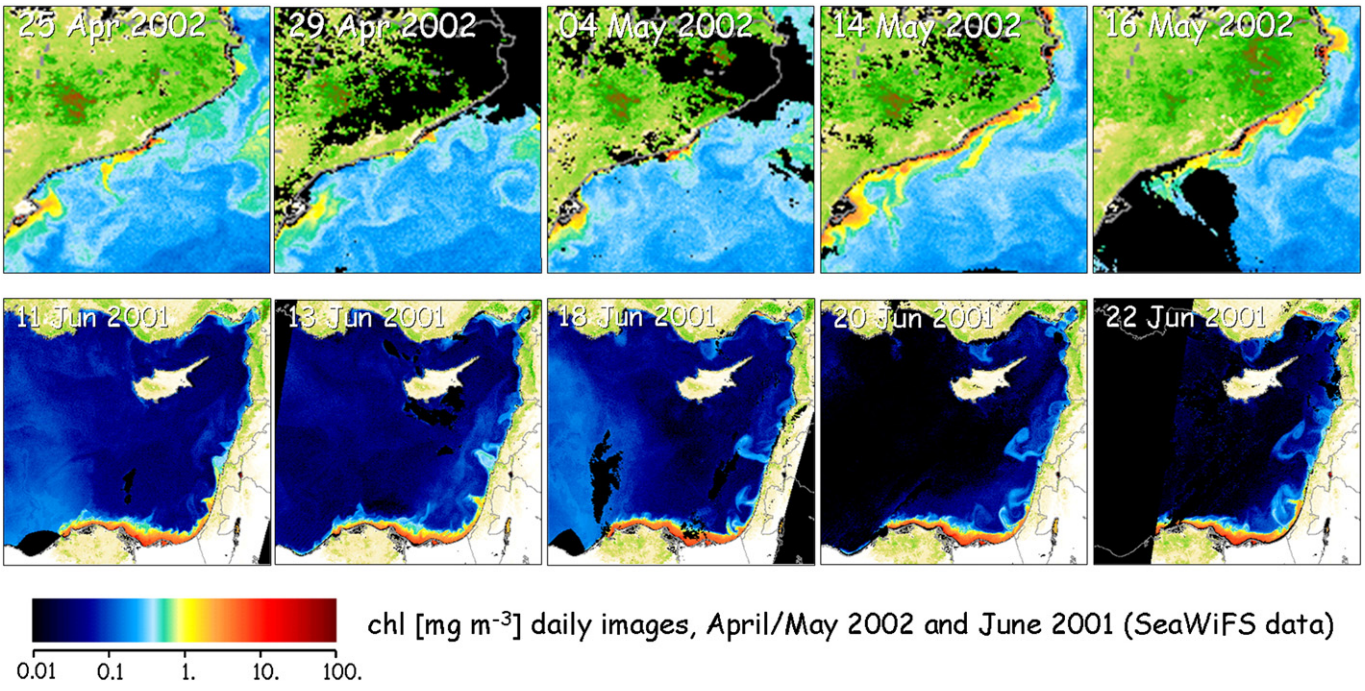

Fig. 12. Selected SeaWiFS-derived *chl* daily images, north-western near-coastal area (upper row, from left to right: 25–29 April and 4-14-16 May, 2002) and south-eastern near-coastal area (lower row, from left to right: 11-13-18-20-22 June, 2001) of the Mediterranean Sea.

rather than lower, than that of surrounding waters (Barale et al., 2005). Among these features, the Nile river plume is by far the main one likely to provide a constant source of nutrients of continental origin. Although the Nile's impact on the pelagic environment has been much reduced by the construction of the Aswan High Dam (Halim et al., 1995), a significant concentration of water constituents still characterize the area surrounding the delta (see Fig. 12). Turbulent diffusion from this area, and from the coastal zone downstream from the delta, with respect to the prevailing cyclonic circulation of the Levantine basin (Alhammoud et al., 2005), is traced by the *chl* field, with various plumes extending offshore. Such a mechanism for biological enrichment of the eastern Mediterranean, supplying nutrients of coastal origin to the primary producers that sustain the food web in this otherwise oligotrophic region — nutrients that originate from an increasing use of fertilizers for agriculture, as well as from the proliferation of untreated sewage outfalls, due to population growth along the coast (Nixon, 2003) — has been suggested as the reason for the recovery of local fisheries, which had collapsed in the mid 1960's after the Nile damming (Bebars et al., 1997; Nixon, 2004).

4. Conclusion

Phytoplankton growth patterns in the Mediterranean Sea have been studied by assessing the SeaWiFS-derived (1998–2003) *chl* indicator, its recurrent patterns as well as its anomalies, at various space and time scales. The climatological *chl* field provides a (background) picture of the ecosystem status, resulting from algal blooms evolution and related environmental boundary conditions. The approach adopted here suggests the hypothesis of a relationship between geographic and climatic factors and bio-geo-chemistry of the basin. The mechanisms of fertilization of the basin, supporting recurrent or anomalous blooming, appear to be ruled mainly by coastal interactions and atmospheric forcing, and then by the ensuing thermohaline processes. Therefore, ecosystem dynamics would seem to be determined primarily by the key morphological and meteorological features of the basin, upon which may (in near-coastal areas) or may not (in the open sea) be superimposed an anthropogenic impact. The ecosystem trends emerging from the analysis of *chl* anomalies point out the main deviations from the background status that occur in the Mediterranean Sea, as well as the hotspots where they seem to recur. Although the general trend between 1998 and 2003 appears to be one of decreasing anomalies, in line with a decrease of the *chl* average basin value, some areas seem to follow an opposite tendency. Most notably, near-coastal areas in the south-eastern and in the north-western parts of the basin display intense local blooms shaped as filaments and eddies. The observable inshore events appear to co-vary with the offshore patterns, but to develop primarily as independent features along the innermost coastal area. When these near-coastal features do interact with the larger basin-wide patterns, they seem to do so extending seaward from the coast, and not to develop under the impact of phenomena taking place in open waters.

Although the time series considered here is too short to provide any indication about long-term trends, the available data set indicates a decrease of *chl* average basin value, over a multi-annual period. Given that phytoplankton growth in the Mediterranean Sea is always nutrient-limited, as in the classical sub-tropical basin scenario, and that vertical mixing is the main mechanism for the fertilization of surface waters with nutrients from deeper layers, then the lower *chl* values point to a more severe nutrient-limitation, due to a more stable water column. This would be the case if indeed the mean temperature of the Mediterranean Sea were increasing, at least since the 1980's, as indicated by much evidence presented in the recent literature on this subject (Bétoux et al., 1998; Lelieveld et al., 2002). A higher surface temperature would mean a stronger stratification of the water column. The ensuing reduced vertical mixing would reduce nutrient fluxes from deep waters and, as a consequence, production in surface waters. Furthermore, the increased stability of the water column would reduce the intensity of anomalous blooms over the basin interior, where nutrient input is from deep layers, and augment it in selected near-coastal areas, where the nutrient input is from continental freshwater spreading over the surface layer (as observed in the present analysis of *chl* anomalies). By the same token, it would also imply not only a strengthening, but also an anticipated onset of the stratification, allowing therefore the spring bloom in the north-western basin to occur earlier in the seasonal cycle (as suggested in the comparison of the CZCS and SeaWiFS *chl* climatologies, in which the bloom — thought to depend on the stabilization of the water column — indeed appears to be anticipated from April to March).

The recurrent, increasing blooms at the various hotspots, appearing in the *chl* anomalies, have been described as localized phenomena, linked to either air–sea interactions in pelagic domain (Lion Gyre and Rhodes Gyre), or increased nutrient availability and low water renewal in coastal areas. The latter kind of anomalous blooms would be related to the anthropogenic impact on coastal sites (*e.g.* crowded beaches or marinas) or to the combination of specific geographical and meteorological conditions (*e.g.* enclosed bays during summer, when hydrodynamic forcing is low). This would suggest that noxious, or harmful, blooms — known to have occurred in the areas and periods considered — are predominantly local phenomena, with little or no connection to regional events. Indeed, the isolated blooms at coastal stations in late winter and early spring, reported in the literature *e.g.* for the Catalan coast (Vila et al., 2005), coincide only occasionally with the regional type of blooming seen in SeaWiFS imagery (possibly reflecting the different forcing functions, acting at different scales, of the two cases, local and regional). Later on in the year, in offshore waters — where thermal stratification progresses and the surface layer becomes nutrient depleted, with possible development of a deep chlorophyll *maximum* — the large-scale, regional blooms seen in the satellite imagery fade away. To the contrary, the stabilization of inshore waters — where nutrient concentration may be quite constant, for the entire annual cycle — continues to favor the growth of smaller-scale phytoplankton populations. Thus, in summer, many coastal blooms can continue to occur, in the surface layer, even though not necessarily at scales accessible to the remote sensing tools used here.

Acknowledgements

The research described in the present paper has been undertaken in the frame of Collaboration Agreement N. 21698-2004-02 S0SC ISP CH between the Institute for Environment and Sustainability (IES), Joint Research Centre (JRC) of the European Commission (EC), and the University of Geneva, Section of Earth Sciences, Remote Sensing and GIS Unit. This joint programme, named "Bio-optical Environmental Assessments of Marginal Seas", was conducted at the IES, JRC EC, within the FP6 Action 2121 ECOMAR, and at the University of Geneva, as part of the internship activities of Barbara Weber, Karin Allenbach and Anaïs Hoareau, whose contribution to the results obtained by this study is gratefully acknowledged. The authors are greatly indebted to Frédéric Melin, IES, JRC EC, for his stewardship in the production, maintenance and provision of the SeaWiFS data set used here. Thanks are also due to four anonymous reviewers, for their helpful suggestions.

References

Alhammoud, B., Béranger, K., Mortier, L., Crépon, M., & Dekeyser, I. (2005). Surface circulation of the Levantine Basin: Comparison of model results with observations. *Progress in Oceanography*, *66*, 299–320.

Alvain, S., Moulin, C., Dandonneau, Y., & Bréon, F. M. (2005). Remote sensing of phytoplankton groups in case 1 waters from global SeaWiFS imagery. *Deep Sea Research*, *I 52*, 1989–2004.

Antoine, D., Morel, A., & André, J. M. (1995). Algal pigment distribution and primary production in the eastern Mediterranean as derived from Coastal Zone Color Scanner observations. *Journal of Geophysical Research*, *100*, 16193–16209.

Arnone, R. A., Wiesenburg, D. A., & Saunders, K. D. (1990). The origin and characteristics of the Algerian Current. *Journal of Geophysical Research*, *95*, 1587–1598.

Artegiani, A., Bregant, D., Paschini, E., Pinardi, N., Raicich, F., & Russo, A. (1997). The Adriatic Sea general circulation. Part I: Air–sea interactions and water mass structure. *Journal of Physical Oceanography*, *27*, 1492–1514.

Artegiani, A., Bregant, D., Paschini, E., Pinardi, N., Raicich, F., & Russo, A. (1997). The Adriatic Sea general circulation. Part II: Baroclinic circulation structure. *Journal of Physical Oceanography*, *27*, 1515–1532.

Baith, K., Lindsay, R., Fu, G., & McClain, C. R. (2001). SeaDAS, a data analysis system for ocean-color satellite sensors. *EOS Transactions AGU*, *82*, 202.

Barale, V. (2003). Environmental remote sensing of the Mediterranean Sea. *Journal of Environmental Science and Health*, *A38*(8), 1681–1688.

Barale, V., Jaquet, J. M., Allenbach, K., Ndiaye, M., & Hoareau, A. (2005). *Bio-optical Environmental Assessments of Marginal Seas. Progress Report 2* (pp. 64). Ispra: European Commission (I), EUR 21899 EN. Available at http://ies.jrc.cec.eu.int/documentation.html or through the Contact Point therein.

Barale, V., & Larkin, D. J. (1998). Optical remote sensing of coastal plumes and run-off in the Mediterranean region. *Journal of Coastal Conservation*, *4*, 51–68.

Barale, V., Larkin, D. J., Fusco, L., Melinotte, J. M., & Pittella, G. (1999). OCEAN Project: the European archive of CZCS historical data. *International Journal of Remote Sensing*, *20*(7), 1201–1218.

Barale, V., McClain, C. R., & Malanotte-Rizzoli, P. (1986). Space and time variability of the surface color field in the northern Adriatic Sea. *Journal of Geophysical Research*, *91*, 12957–12974.

Barale, V., Weber, B., & Jaquet, J. M. (2004). *Bio-optical Environmental Assessments of Marginal Seas. Progress Report 1* (pp. 50). Ispra: European Commission (I), EUR 21479 EN. Available at http://ies.jrc.cec.eu.int/documentation.html or through the Contact Point therein.

Barale, V., & Zin, I. (2000). Impact of continental margins in the Mediterranean Sea: hints from the surface colour and temperature historical record. *Journal of Coastal Conservation*, *6*, 5–14.

Barnes, R.A., Eplee, R.E. Jr., Biggar, S.F., Thome, K.J., Zalewski, E.F., Slater, P.N., et al. (1999a). The SeaWiFS Solar Radiation-Based Calibration and the Transfer-to-Orbit Experiment. Vol. 5, NASA Technical Memorendum 1999–206892.

Barnes, R. A., Eplee, R. E., Jr., Patt, F. S., & McClain, C. R. (1999). Changes in the radiometric sensitivity of SeaWiFS determined from lunar and solar-based measurements. *Applied Optics*, *38*, 4649–4664.

Bebars, M. I., Lasserre, G., & Lam Hoai, T. (1997). Analyse des captures des pêcheries marines et lagunaires d'Egypte en liaison avec la construction du haut barrage d'Assouan. *Oceanologica Acta*, *20*, 421–436.

Berland, B. R., Bonin, D. J., & Mestrini, S. Y. (1980). Azote ou phosphore? Considérations sur le "paradoxe nutritionnel" de la Mer Méditerranée. *Oceanologica Acta*, *3*, 135–142.

Berthon, J. F., & Zibordi, G. (2004). Bio-optical relationships for the northern Adriatic Sea. *International Journal of Remote Sensing*, *25*(7–8), 1527–1532.

Bétoux, J. -P., Gentili, B., & Tailliez, D. (1998). Warming and freshwater budget change in the Mediterranean since the 1940s, their possible relation to the greenhouse effect. *Geophysical Research Letters*, *25*(7), 1023–1026.

Bosc, E., Bricaud, A., & Antoine, D. (2004). Seasonal and interannual variability in algal biomass and primary production in the Mediterranean Sea, as derived from 4 years of SeaWiFS observations. *Global Biogeochemical Cycles*, *18*, GB1005. doi:10.1029/2003GB002034.

Bricaud, A., Bosc, E., & Antoine, D. (2002). Algal biomass and sea surface temperature in the Mediterranean basin: Intercomparison of data from various satellite sensors, and implications for primary production estimates. *Remote Sensing of Environment*, *81*, 163–178.

Bulgarelli, B., & Mélin, F. (2000). *SeaWiFS Data Processing Code, REMBRANDT v. 1, Code Elements* (pp. 27). Ispra: European Commission (I), EUR 19514 EN. Available at http://ies.jrc.cec.eu.int/documentation.html or through the Contact Point teherein.

Bulgarelli, B., Zibordi, G., & Mélin, F. (2002). *SeaWiFS Data Processing Code REMBRANDT: Accuracy Evaluation of the Atmospheric Correction Method* (pp. 12). Ispra: European Commission (I), EUR 20533 EN. Available at http://ies.jrc.cec.eu.int/documentation.html or through the Contact Point teherein.

Claustre, H., Morel, A., Hooker, S. B., Babin, M., Antoine, D., Oubelkheir, K., et al. (2002). Is desert dust making oligotrophic waters greener? *Geophysical Research Letters*, *29*(10). doi:10.1029/2001GL014056.

Corsini, G., Grasso, R., & Cipollini, P. (2002). Regional bio-optical algorithms for the Alboran Sea from a reflectance model and in situ data. *Geophysical Research Letters*, *29*(15), 1739. doi:10.1029/2001GL013861.

Darzi, M. (1998). SeaWiFS science algoritm flow chart. *NASA Technical Memorandum*, 1998–206848.

D'Ortenzio, F., Marullo, S., Ragni, M., Ribera d' Alcalá, M., & Santoleri, R. (2002). Validation of empirical SeaWiFS algorithms for chlorophyll-α retrieval in the Mediterranean Sea. A case study for oligotrophic seas. *Remote Sensing of Environment*, *82*(1), 79–94.

D'Ortenzio, F., Iudicone, D., de Boyer Montegut, C., Testor, P., Antoine, D., Marullo, S., et al. (2005). Seasonal variability of the mixed layer depth in the Mediterranean Sea as derived from in situ profiles. *Geophysical Research Letters*, *32*, L12605. doi:10.1029/2005GL022463.

EEA (2006). Priority issues in the Mediterranean environment. *European Environment Agency Report No. 4/2006* (pp. 86). Copenhagen: EEA.

EEA (2006). The changing faces of Europe's coastal areas. *European Environment Agency Report No. 6/2006* (pp. 107). Copenhagen: EEA.

Forcada, J., Aguilar, A., Hammond, P., Pastor, X., & Aguilar, R. (1996). Distribution and abundance of fin whales in the western Mediterranean Sea during summer. *Journal of Zoology*, *238*, 23–34.

Fredj, G., Bellan Santini, D., & Meinardi, M. (1992). Etat des connaissances sur la faune marine Méditerranéenne. *Bulletin de l'Institut Oceanographique, Monaco, Numéro Spécial*, *9*, 135–145.

Garcés, E., Masó, M., Vila, M., & Camp, J. (2000). HAB events in the Mediterranean Sea: are they increasing? A case study of the last decade in the NW Mediterranean and the genus Alexandrium. *Harmful Algal News*, *20*, 1–11.

Gascard, J. C. (1973). Vertical motions in a region of deep water formation. *Deep Sea Research*, *20*, 1011–1027.

Gascard, J. C. (1978). Mediterranean deep water formation, baroclinic instability and oceanic eddies. *Oceanologica Acta*, *1*(3), 315–330.

Gitelson, A., Karnieli, A., Goldman, N., Yacobi, Y. Z., & Mayo, M. (1996). Chlorophyll estimation in the south-eastern Mediterranean using CZCS images: Adaptation of an algorithm and its validation. *Journal of Marine Systems*, *9*, 283–290.

Gregg, W. W., & Casey, N. W. (2004). Global and regional evaluation of the SeaWiFS chlorophyll data set. *Remote Sensing of Environment*, *93*(4), 463–479.

Guerzoni, S., Chester, R., Dulac, F., Herut, B., Loye-Pilot, M. D., Measures, C., et al. (1999). The role of atmospheric deposition in the biogeochemistry of the Mediterranean Sea. *Progress in Oceanography*, *44*, 147–190.

Halim, Y. S., Morcos, A., Rizkalla, S., & El-Sayed, M. Kh. (1995). The impact of the Nile and the Suez Canal on the living marine resources of the Egyptian Mediterranean waters (1958–1986). *FAO Fisheries Technical Paper*, *349*, 19–57.

IOCCG (2000). Remote sensing of ocean colour in coastal, and other optically-complex, waters. In S. Sathyendranath (Ed.), *Reports of the International Ocean-Colour Coordinating Group, No. 3* (pp. 140). Darthmouth: IOCCG.

Jaquet, J. M., Tassan, S., Barale, V., & Sarbaji, M. (1999). Bathymetric and bottom effects on CZCS chlorophyll-like pigment estimation: data from the Kerkennah shelf (Tunisia). *International Journal of Remote Sensing*, *20*(7), 1343–1362.

Lelieveld, J., Berresheim, H., Borrmann, S., Crutzen, P. J., Dentener, F. J., Fischer, H., et al. (2002). Global air pollution crossroads over the Mediterranean. *Science*, *298*, 794–799.

Levy, M., Memery, L., & Madec, G. (1998). The onset of a bloom after deep winter convection in the northwestern Mediterranean Sea: Mesoscale process study with a primitive equation model. *Journal of Marine Systems*, *16*(1–2), 7–21.

Levy, M., Memery, L., & Madec, G. (1999). The onset of the spring bloom in the MEDOC area: mesoscale spatial variability. *Deep Sea Research, Part I — Oceanographic Research Papers*, *46*(7), 1137–1160.

Levy, M., Memery, L., & Madec, G. (2000). Combined effects of mesoscale processes and atmospheric high-frequency variability on the spring bloom in the MEDOC area. *Deep Sea Research, Part I — Oceanographic Research Papers*, *47*(1), 27–53.

Mann, K. H., & Lazier, J. R. N. (2006). *Dynamics of Marine Ecosystems: Biological–Physical Interactions in the Oceans* (pp. 496)., Third edition Malden, MS: Blackwell Publishing.

McClain, C. R., Feldman, G. C., & Hooker, S. B. (2004). An overview of the SeaWiFS project and strategies for producing a climate research quality global ocean bio-optical time series. *Deep Sea Research, II*, *51*, 5–42.

MEDOC Group (1970). Observations of deep water in the Mediterranean Sea. *Nature*, *227*, 1037–1040.

Mélin, F., Bulgarelli, B., Gobron, N., Pinty, B., & Tacchi, R. (2000). *An integrated tool for SeaWiFS operational processing* (pp. 33). Ispra: European Commission (I), EUR 19576 EN. Available at http://ies.jrc.cec.eu.int/documentation.html or through the Contact Point therein.

Millot, C., & Taupier-Letage, I. (2005). Circulation in the Mediterranean sea. In A. Saliot (Ed.), *The Mediterranean Sea, Handbook of Environmental Chemistry, V. 5 Water Pollution, Part K* (pp. 29–66). Berlin, Heidelberg: Springer–Verlag.

Morel, A., & André, J. M. (1991). Pigment distribution and primary production in the western Mediterranean as derived and modeled from Coastal Zone Color Scanner observations. *Journal of Geophysical Research*, *96*, 12685–12698.

Nixon, S. W. (2003). Replacing the Nile: Are anthropogenic nutrients providing the fertility once brought to the Mediterranean by a great river? *Ambio*, *32*, 30–39.

Nixon, S. W. (2004). The Artificial Nile. *American Scientist*, *92*, 158–165.

O'Reilly, J. E., Maritorena, S., Mitchell, B. G., Siegel, D. A., Carder, K. L., Garver, S. A., et al. (1998). Ocean color chlorophyll algorithms for SeaWiFS. *Journal of Geophysical Research*, *103*, 24937–24953.

Ouillon, S., & Petrenko, A. A. (2005). Above-water measurements of reflectance and chlorophyll-*a* algorithms in the Gulf of Lions, NW Mediterranean Sea. *Optics Express*, *13*(7), 2531–2548.

Robinson, A. R., & Golnaraghi, M. (1995). The physical and dynamical oceanography of the Mediterranean Sea. In P. Malanotte Rizzoli, & A. R. Robinson (Eds.), *Ocean Processes in Climate Dynamics: Global and Mediterranean Examples* (pp. 255–306). New York: Springer.

Smith, R. C. (1981). Remote sensing and depth distribution of ocean chlorophyll. *Marine Ecology Progress Series*, *5*, 359–361.

Sturm, B., Barale, V., Larkin, D., Andersen, J. H., & Turner, M. (1999). OCEANcode: the complete set of algorithms and models for the level-2 processing of European CZCS historical data. *International Journal of Remote Sensing*, *20*(7), 1219–1248.

Sturm, B., & Zibordi, G. (2002). SeaWiFS atmospheric correction by an approximate model and vicarious calibration. *International Journal of Remote Sensing*, *23*(3), 489–501.

Vila, M., Garcés, E., Masó, M., & Camp, J. (2001). Is the distribution of the toxic dinoflagellate Alexandrium catenella expanding along the North West Mediterranean coast? *Marine Ecology Progress Series*, *222*, 73–83.

Vila, M., Giacobbe, M. G., Masó, M., Gangemi, E., Penna, A., Sampedro, N., et al. (2005). A comparative study on recurrent blooms of *Alexandrium minutum* in two Mediterranean harbors. *Harmful Algae*, *4*, 673–695.

Vila, M., & Masó, M. (2005). Phytoplankton functional groups and harmful species in anthropogenically impacted waters of the NW Mediterranean Sea. *Scientia Marina*, *69*, 31–45.

Volpe, G., Santoleri, R., Vellucci, V., Ribera d'Alcalá, M., Marullo, S., & D'Ortenzio, F. (2007). The colour of the Mediterranean Sea: Global versus regional bio-optical algorithms evaluation and implication for satellite chlorophyll estimates. *Remote Sensing of Environment*, *107*(4), 625–638.

Weber, B., Jaquet, J. M., & Faour, G. (2004). Cartographie et origine des panaches chlorophylliens côtiers en Méditerrannée orientale à partir des images de SeaWiFS et d'ETM+ de Landsat 7. *Télédétection*, *4*(2), 175–195.

Zecchetto, S., & Cappa, C. (2001). The spatial structure of the Mediterranean Sea winds revealed by ERS-1 scatterometer. *International Journal of Remote Sensing*, *22*(1), 45–70.

Zibordi, G., Mélin, F., & Berthon, J. -F. (2006). A time series of above-water radiometric measurements for coastal water monitoring and remote sensing product validation. *IEEE Geoscience Remote Sensing Letters*, *3*, 120–124. doi:10.1109/LGRS.2005.858486.